中國機械工程學刊第四十二卷第六期第 539~550 頁(民國一百一十年)
Journal of the Chinese Society of Mechanical Engineers, Vol.42, No.6, pp. 539~550 (2021)

Nanoindentation Behaviour of As-Deposited and Annealed SiO_2/GaAs Thin Films

Woei-Shyan Lee* and Wilbert Chu **

Keywords: Nanoindentation, GaAs, Microstructural evolution, Annealing, SiO_2 Thin films

ABSTRACT

SiO_2 thin films with thicknesses of 200 nm and 300 nm, respectively, are deposited on GaAs substrates. The mechanical properties of the SiO_2/GaAs thin-film systems are evaluated under room temperature (RT) conditions by nanoidentation tests performed to depths ranging from 150 to 350 nm. The tests are performed using both as-deposited samples and samples annealed at 500 ℃ for 30 minutes. The results show that for the as-deposited specimens, a pop-in effect occurs in the loading curve for all film thicknesses and nanoindentation depths (150 nm and 350 nm) due to delamination of the thin film from the substrate. However, for the annealed samples, no pop-in events are observed, irrespective of the film thickness or nanoindentation depth. For both samples (as-deposited and annealed), the maximum indentation load increases with an increasing indentation depth and film thickness. However, the shape of the hardness-depth curve for the annealed specimens is different from that of the as-deposited specimens. Moreover, the hardness of the annealed specimens is slightly less than that of the as-deposited specimens at the maximum indentation depth. Similar tendencies can be observed for the variation of Young's modulus with the indentation depth. Scanning electron microscopy (SEM) observations show that the indentation area increases with an increasing indentation depth and thin film thickness, but decreases in the annealed condition. The transmission electron microscopy (TEM) observations reveal that no delamination occurs for the annealed specimen with the maximum thickness of 300 nm under indentation depths of 150 nm and 350 nm. In addition, dislocations within the GaAs substrate are apparent only in the annealed specimen with a thickness of 300 nm and an indentation depth of 350 nm.

The selected area (electron) diffraction (SAED) patterns confirm that the as-deposited and annealed SiO_2 film has an amorphous structure, while the GaAs substrate has a single crystal structure. Finally, the high-resolution TEM (HRTEM) micrographs show that the as-deposited and annealed GaAs substrate has lattice spacing of 0.283 nm while there is none for SiO_2 since it has an amorphous structure.

Paper Received October 2021. Revised November, 2021, Accepted December, 2021, Author for Correspondence: Woei-Shyan Lee.

** Distinguished Professor, Department of Mechanical Engineering, National Cheng Kung University, Tainan, Taiwan 70101, ROC.*

*** Graduate Student, Department of Mechanical Engineering, National Cheng Kung University, Tainan, Taiwan 70101, ROC.*

INTRODUCTION

Gallium arsenide (GaAs) has high electron mobility and drift velocity, a high band-gap, and good thermal stability. As a result, it is widely used in the fabrication of displays, sensors, light-emitting diodes (LEDs), and solar cells (Yugang *et al*, 2005; Nakamura, 2012). For solar cell applications, the deposition of a thin layer of SiO_2 on the GaAs surface can enhance the conversion efficiency to achieve a highly absorbent surface (Electrochem, 2014; Zhang *et al*, 2019). However, to ensure the robustness of the SiO_2/GaAs structure during the panel fabrication process, the mechanical properties of the SiO_2/GaAs thin-film system must be properly understood.

The literature contains many studies on the mechanical properties of GaAs during nanoindentation. In general, these studies have shown that GaAs undergo plastic deformation under the effects of the indentation load (Leipner *et al.*, 2001). However, the effects of the annealing temperature on the plastic deformation of nanoindented SiO_2/GaAs thin films are still unclear. Many studies have shown the existence of a discontinuity (pop-in) phenomenon in the loading curve of GaAs and other semiconductors (Leipner *et al.*, 2001; Chrobak *et al.*, 2007). These discontinuities have been variously ascribed to the deformation of dislocations, plastic deformation, and buckling phenomena under the action of the indenter (Patriarche *et al.*, 2004). For solar cell applications, the structural discontinuities may result in significant changes to the mechanical and electrical properties. Consequently, the origins and effects of these discontinuities must be properly understood.

Therefore, this study investigates the mechanical properties (i.e., hardness and Young's modulus) of two SiO_2/GaAs thin-film systems with thicknesses of 200 nm and 300 nm, respectively, under nanoindentation depths in the range of 150 to 350 nm.

The nanoindentation tests are performed using both as-deposited samples and specimens annealed at a temperature of 500℃ for 30 minutes. The effects of the thin-film thickness, indentation depth and annealing process on the mechanical properties of the SiO_2/GaAs thin films are clarified by means of scanning electron microscopy (SEM) and transmission electron microscopy (TEM) observations. Finally, the crystal structures and lattice spacings of the as-deposited and annealed nanoindented SiO_2/GaAs structures are examined via selected area (electron) diffraction (SAED) analysis and high-resolution TEM (HRTEM).

THEORETICAL BACKGROUND OF NANOINDENTATION TESTS

In nanoindentation tests, Young's modulus is generally evaluated using the Oliver and Pharr model, which has the form (Timoshenko and Goodier, *1951*; Pharr *et al*, 1992)

$$\frac{1}{E_r}=\frac{(1-\nu_s^{\,2})}{E_s}+\frac{(1-\nu_i^{\,2})}{E_i} \tag{1}$$

where E_s and E_i are the elastic modulus values of the specimen and indenter, respectively; V_s and V_i are the Poisson ratios of the specimen and indenter, respectively; and E_r is the reduced modulus. Note that E_r accounts for the elastic deformation of the indenter, and is defined as

$$E_r=\frac{\sqrt{\pi}}{2}\frac{S}{\sqrt{A}} \tag{2}$$

where *S* is the contact stiffness (i.e., the slope of the load-displacement curve at the beginning of the unloading phase) and *A* is the projected contact area. The contact stiffness is derived as

$$S=\left.\frac{dP}{dh}\right|_{h_{\max}} \tag{3}$$

where *h* is the total displacement of the center of the probe from the surface. Defining h_c as the contact depth, i.e., the vertical depth over which the probe contacts the specimen, and h_s as the surface depth, i.e., the vertical depth over which the probe does not contact the surface, *h* can be defined mathematically as

$$h=h_s+h_c \tag{4}$$

Under the assumption of elastic deformation, the loading force and probe displacement during the unloading stage are related by the following power law equation:

$$P=\alpha(h-h_f)^m \tag{5}$$

Where *P* is the loading force, $h-h_f$ is the elastic displacement of the probe, and α and *m* are constants derived by curve fitting the following equation:

$$S=\left(\frac{dP}{dh}\right)_{h_{\max}}=\alpha m(h_{\max}-h_f)^{m-1} \tag{6}$$

The hardness of the sample can be obtained by dividing the maximum normal indentation load, P_{max} by the projected area of the contact depth A, i.e.,

$$H=\frac{P_{\max}}{A} \tag{7}$$

where A is determined from the area function $A(h_c)$, which expresses the cross-sectional area of the indenter in terms of the contact depth. The actual depth of contact (h_c) is determined as

$$h_c=h_{\max}-\varepsilon\frac{P_{\max}}{S} \tag{8}$$

where h_{max} is the maximum penetration depth of the indenter, ε is a geometrical constant associated with the indenter shape (e.g., $\varepsilon=0.75$ for a Berkovich indenter), and S is the contact stiffness.

Having computed h_c, the projected contact area A can be determined from the following fitting equation (Oliver and Pharr, 1992)

$$A=f(h_c)=24.5h_c^2+c_1h_c^1+c_2h_c^{1/2}+c_3h_c^{1/4}+\ldots+c_8h_c^{1/128} \tag{9}$$

where C_1 through C_8 are constants. Note that the first term on the right-hand side of Eq. (9) describes a perfect Berkovich indenter, while the other terms describe the deviations of the actual indenter geometry from the ideal Berkovich geometry due to tip blunting.

If the probe geometry is not axisymmetric, the reduced modulus given in Eq. (2) should be revised as follows:

$$E_r=\frac{1}{\beta}\frac{\sqrt{\pi}}{2}\frac{S}{\sqrt{A}} \tag{10}$$

where β has a value of 1.034 for a Berkovich probe (Hansen and Anderko, 1958)

SiO_2/GaAs thin films are single-film coated systems with a composite structure. Consequently, the Young's modulus of the film is determined by both the Young's modulus of the SiO_2 film and the Young's modulus of the GaAs substrate. In other words, the Young's modulus E_f of the combined film/substrate system can be estimated as (Huajian *et al.*, 1992)

$$\frac{1}{E_r}=\frac{1-\nu_i^{\,2}}{E_i}+\frac{1-\nu_f^{\,2}}{E_f}(1-e^{-\alpha\frac{t}{a}})+\frac{1-\nu_s^{\,2}}{E_s}e^{-\alpha\frac{t}{a}} \tag{11}$$

where E_s is the Young's modulus of the bulk gallium arsenide substrate, and E_r is the reduced modulus. Furthermore, V_s, V_i and V_f are the Poisson ratios of the specimen, indenter and film, respectively;

and t is the depth under the indenter. Finally, $a = \sqrt{A}$ and α is a constant relating to the probe geometry.

EXPERIMENTAL PROCEDURE

The TEM foil was prepared by using the Hitachi NX2000 advanced triple focused ion milling (FIB) system with a Ga+ ion beam and an operating voltage of 30 keV (see Figure 1). (Note that before the foil is milled, a thin layer of carbon is deposited on the surface of the specimen to protect the indented areas from accidental damage by the ion beam. The cross-sectional microstructures of the various specimens were observed using an EOL JEM-3010 Analytical Scanning Transmission Microscope at 300 kV.

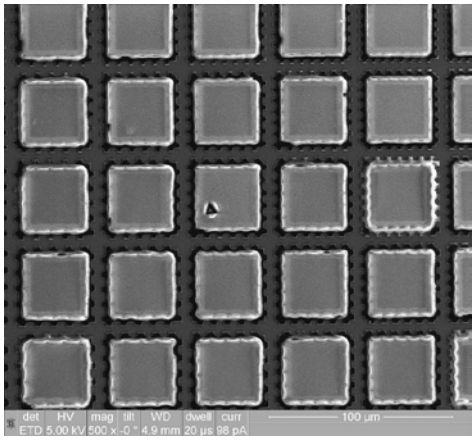

Fig. 1 (a) Original indentation positions identified using scanning electron microscopy and permanent position array system.

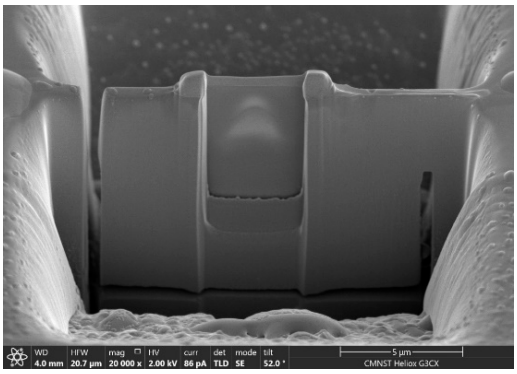

Fig. 1 (b) TEM thin foil specimen prepared using focused ion beam (FIB) milling system.

SiO_2/GaAs specimens were prepared by depositing SiO_2 films with thicknesses of approximately 200 and 300 nm, respectively, on GaAs substrates using a RF-sputtering deposition system. During the deposition process, the substrate was rotated at a speed of 250 rpm and maintained at a temperature of 200 ℃ in order to enhance the uniformity of the deposited film. Following the deposition process, half of the specimens were annealed at 500 ℃ for 30 minutes in a thermal annealing system. Nanoindentation tests were then performed on both the as-deposited samples and the annealed samples using an MTS nanoindenter XP system with a Berkovich diamond pyramid tip. For each sample, the indentation procedure was performed using the following steps: (1) the specimen was indented to a maximum depth of 150 nm or 350 nm; (2) the indenter was held at the point of maximum indentation depth for 10s; and (3) the indenter was smoothly unloaded over a period of 15s. The load-displacement data recorded during each test were used to determine the hardness and Young's modulus of the SiO_2/GaAs thin film in accordance with the Oliver and Pharr method described in (Li and Bhushan, 2002).

RESULTS and DISCUSSION

Loading-unloading curves

Figures 2 (a) and (b) show the load-unloading curves of the as-deposited and annealed specimens, respectively, with a thin film thickness of 200 nm and an indentation depth of 150 nm. A clear pop-in event is seen in the loading curve for the as-deposited specimen (Fig. 2(a)). However, for the annealed specimen, no such effect is observed (Fig. 2(b)).

Figures 2 (c) and (d) show the load-unloading curves of the as-deposited and annealed specimens with the same thin-film thickness of 200 nm but a greater indentation depth of 350 nm. Again, distinct pop-in events are observed in the loading curve of the as-deposited sample, but are absent in the annealed sample.

Figures 3 (a) and (b) show the load-unloading curves of the as-deposited and annealed samples, respectively, with a thin film thickness of 300 nm and an indentation depth of 150 nm. As for the cases shown in Fig. 2, the loading curves of the as-deposited samples show prominent pop-in features for both indentation depths.

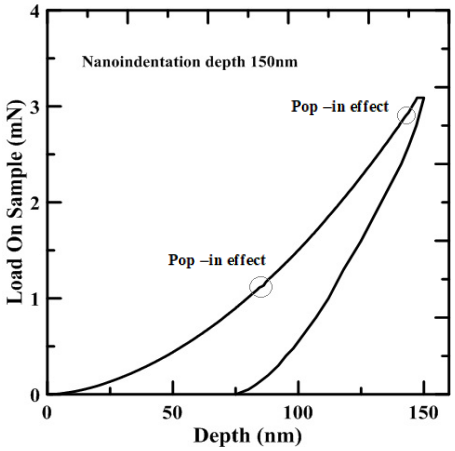

Fig. 2 (a) Load-displacement curves obtained in nanoindentation tests for as-deposited specimen with 200 nm thickness and indentation depth of 150 nm.

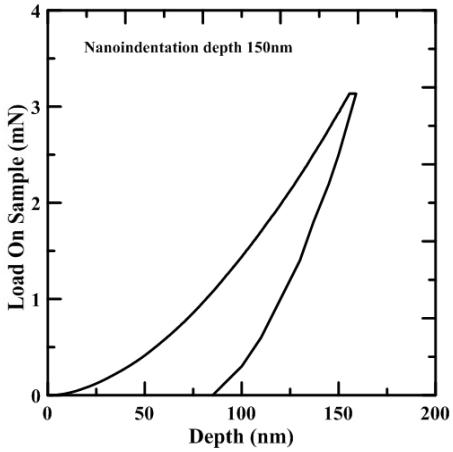

Fig. 2 (b) Load-displacement curves obtained in nanoindentation tests for annealed specimen with 200 nm thickness and indentation depth of 150 nm.

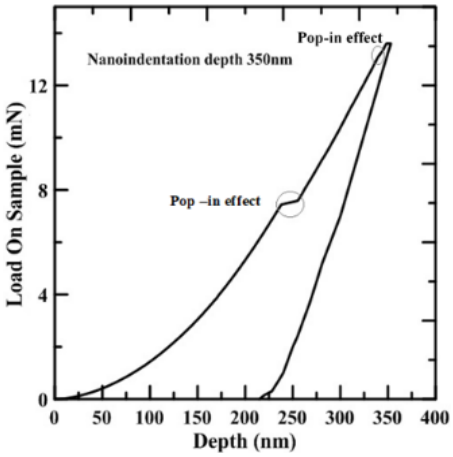

Fig. 2 (c) Load-displacement curves obtained in nanoindentation tests for as-deposited specimen with 200 nm thickness and indentation depth of 350 nm.

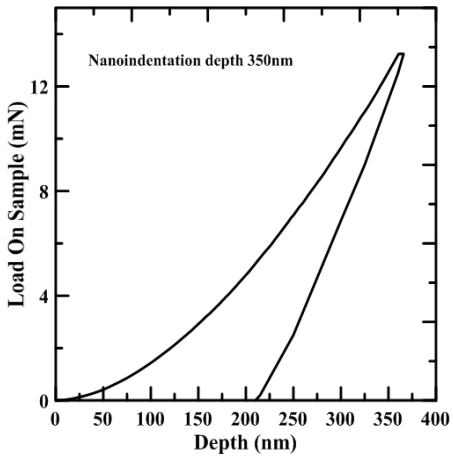

Fig. 2 (d) Load-displacement curves obtained in nanoindentation tests for annealed specimen with 200 nm thickness and indentation depth of 350 nm.

Figures 3 (c) and (d) show the equivalent load-unloading curves for an indentation depth of 350 nm. For the annealed specimens, the loading curves are once again continuous and smooth without any pop-in events. The observed pop-in features in the loading curves have been variously attributed to the generation of dislocations in the substrate (Wasmer *et al.*, 2011), a difference in the mechanical properties of the thin film and substrate, respectively (Haq *et al.*, 2007), and the formation of high-pressure phase in the indentation process.

Comparing the various loading and unloading curves shown in Figs. 2 (a) to 3 (d), it can be observed that for a given film thickness, the maximum load increases with increasing indentation depth. Similarly, for a constant indentation depth, the maximum load increases with an increasing thin film thickness.

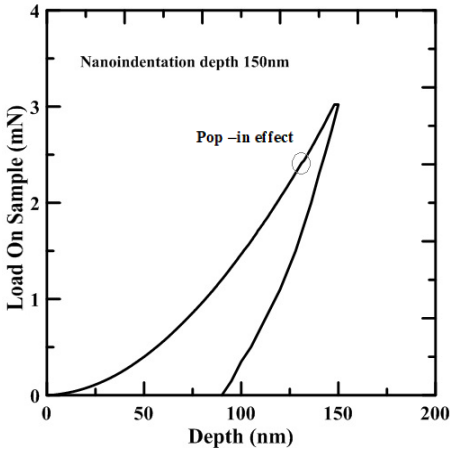

Fig. 3 (a) Load-displacement curves obtained in nanoindentation tests for as-deposited specimen with 300 nm thickness and indentation depth of 150 nm.

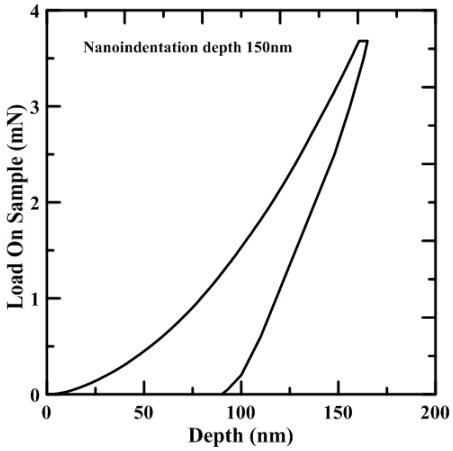

Fig. 3 (b) Load-displacement curves obtained in nanoindentation tests for annealed specimen with 300 nm thickness and indentation depth of 150 nm.

Hardness of SiO_2/GaAs thin films

Figures 4 (a) and (b) show the variation of the SiO_2/GaAs thin film hardness with the indentation depth for the as-deposited and annealed samples, respectively, with a film thickness of 200 nm and an indentation depth of 150 nm. The hardness is unstable

during the initial stages of indentation due to the indentation size effect. However, when the indenter tip is embedded entirely within the GaAs substrate, it stabilizes to an approximately constant value. For the as-deposited specimen (Fig. 4 (a)), the hardness has a final value of around 8.7GPa at the maximum indentation depth of 150 nm. The hardness-depth curve of the annealed specimen differs markedly from that of the as-deposited sample. In particular, the hardness increases sharply to 7.8 GPa (see Fig. 4 (b)), but then reduces rapidly to and then maintains a low and approximately constant value of 5.3GPa as the indentation depth is further increased to 150 nm.

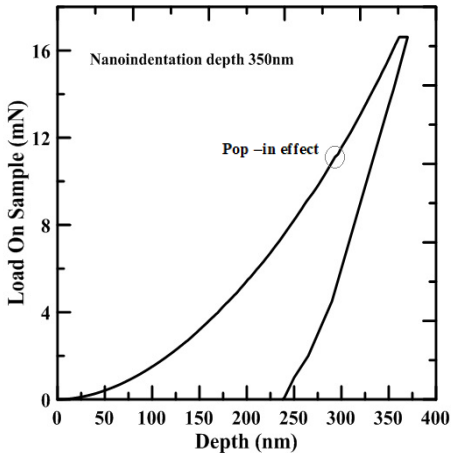

Fig. 3 (c) Load-displacement curves obtained in nanoindentation tests for as-deposited specimen with 300 nm thickness and indentation depth of 350 nm.

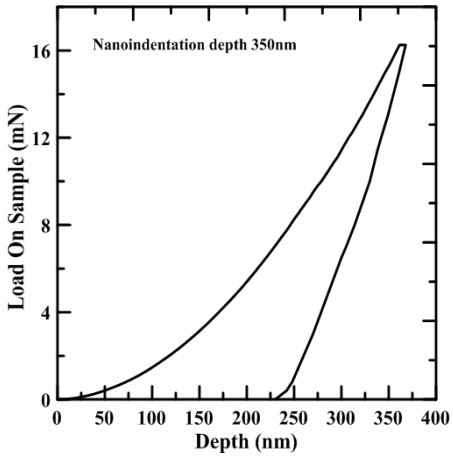

Fig. 3 (d) Load-displacement curves obtained in nanoindentation tests for annealed specimen with 300 nm thickness and indentation depth of 350 nm.

Figures 4 (c) and (d) show variations in the hardness of SiO_2/GaAs thin films with indentation depths for as-deposited and annealed specimens, respectively, with a film thickness of 200 nm and an indentation depth of 350 nm. It is seen that for both samples, the shape and variation tendency of the hardness-depth curve are similar to those of the samples indented to a lower depth of 150 nm (Figs. 4 (a) and (b)). Furthermore, the maximum hardness values of the two samples are also similar to those in Figs. 4 (a) and (b)).

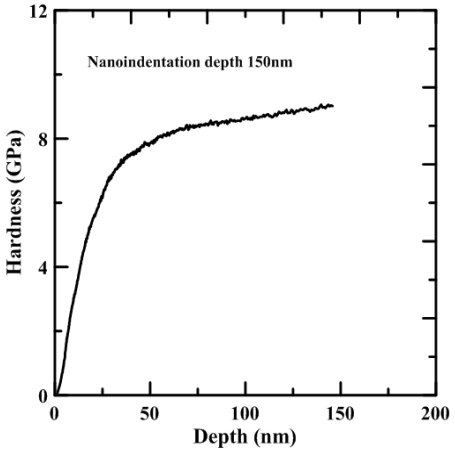

Fig. 4 (a) Hardness-displacement curves obtained in nanoindentation tests for as-deposited specimen with 200 nm thickness and indentation depth of 150 nm.

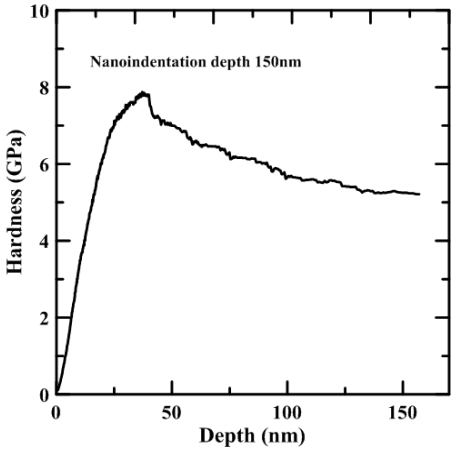

Fig. 4 (b) Hardness-displacement curves obtained in nanoindentation tests for annealed specimen with 200 nm thickness and indentation depth of 150 nm.

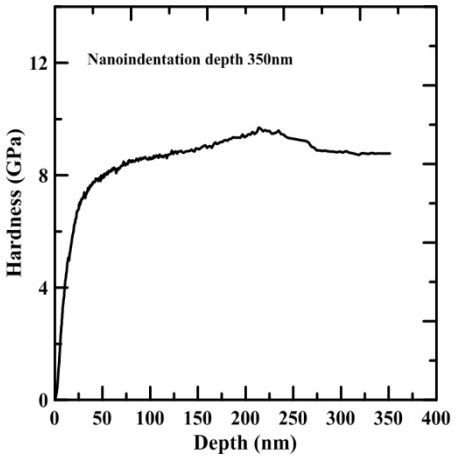

Fig. 4 (c) Hardness-displacement curves obtained in nanoindentation tests for as-deposited specimen with

200 nm thickness and indentation depth of 350 nm.

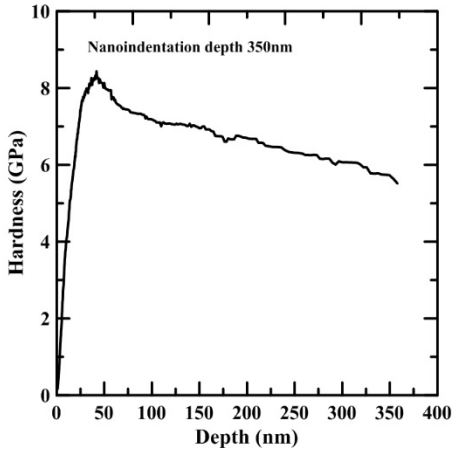

Fig. 4 (d) Hardness-displacement curves obtained in nanoindentation tests for annealed specimen with 200 nm thickness and indentation depth of 350 nm.

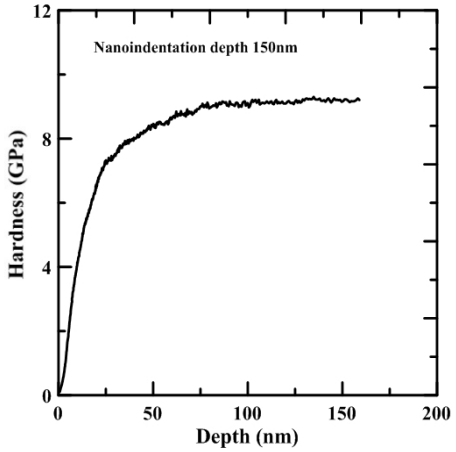

Fig. 5 (a) Hardness-displacement curves obtained in nanoindentation tests for as-deposited specimen with 300 nm thickness and indentation depth of 150 nm.

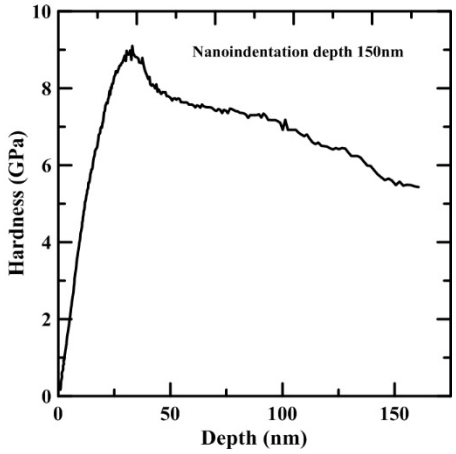

Fig. 5 (b) Hardness-displacement curves obtained in nanoindentation tests for annealed specimen with 300 nm thickness and indentation depth of 150 nm.

Figures 5(a) and (b) show the hardness-depth curves of the as-deposited and annealed samples with a thickness of 300 nm and indentation depth of 150 nm. The maximum hardness values once again look similar to those presented in Fig. 4 for thin films with a lower thickness of 200 nm. Overall, therefore, the results presented in Figs. 4 and 5 show that the maximum hardness of SiO_2/GaAs films is insensitive to the depth of indentation and film thickness. However, for all values of film thickness and indentation depth, the maximum hardness of the annealed sample is lower than that of the as-deposited samples. Figures 5(c) and (d) show the equivalent curves for the samples indented to a greater depth of 350 nm.

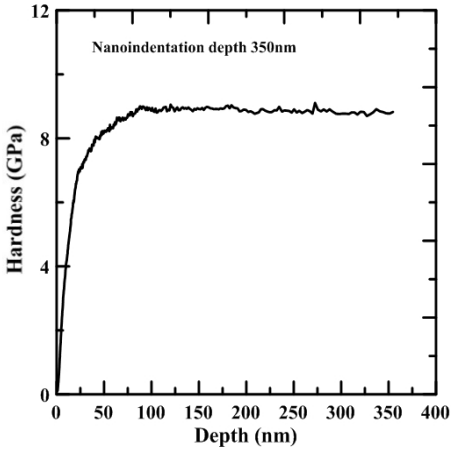

Fig. 5 (c) Hardness-displacement curves obtained in nanoindentation tests for as-deposited specimen with 300 nm thickness and indentation depth of 350 nm.

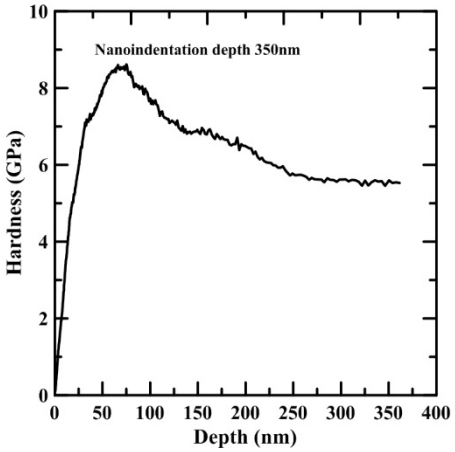

Fig. 5 (d) Hardness-displacement curves obtained in nanoindentation tests for annealed specimen with 300 nm thickness and indentation depth of 350 nm.

Young's modulus of SiO_2/GaAs thin films

Figures 6 (a) and (b) show the variation of the Young's modulus of the as-deposited specimen and annealed specimen, respectively, with a thickness of 200 nm and an indentation depth of 150 nm. It is found that for both samples, the Young's modulus is unstable during the initial stages of indentation due to the indentation size effect (Manika and Maniks, 2006). However, when the indenter tip is embedded entirely

within the GaAs substrate, the Young's modulus stabilizes to an approximately constant value. For the as-deposited specimen (Fig. 6 (a)), the Young's modulus has an unstable value in the initial stage but tends to have a stable value around 74GPa in the later stage as the indentation depth increases to 150 nm. For the annealed specimen (Fig. 6 (b)), the oscillation effect caused by the poorly-calibrated tip area function occurs at a slightly higher indentation depth of 15 nm. As the indenter penetrates more deeply into the SiO_2 film, the Young's modulus increases to a maximum value of approximately 80GPa at an indentation depth of around 28 nm and then falls slowly to a constant value of around 67.4GPa as the indentation depth is further increased to 150 nm.

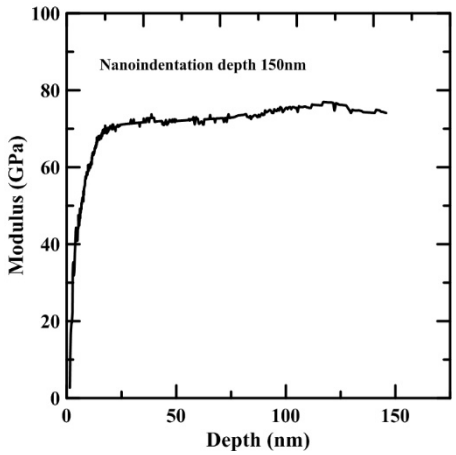

Fig. 6 (a) Modulus-displacement curves obtained in nanoindentation tests for as-deposited specimen with 200 nm thickness and indentation depth of 150 nm.

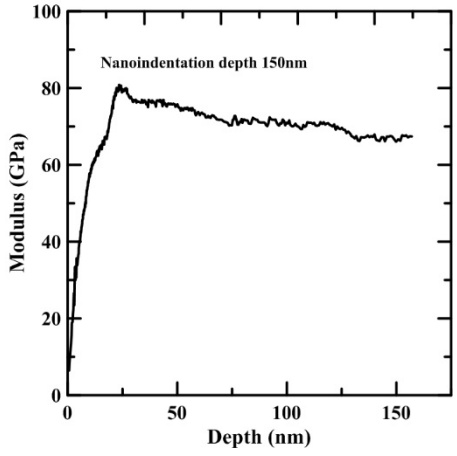

Fig. 6 (b) Modulus-displacement curves obtained in nanoindentation tests for annealed specimen with 200 nm thickness and indentation depth of 150 nm.

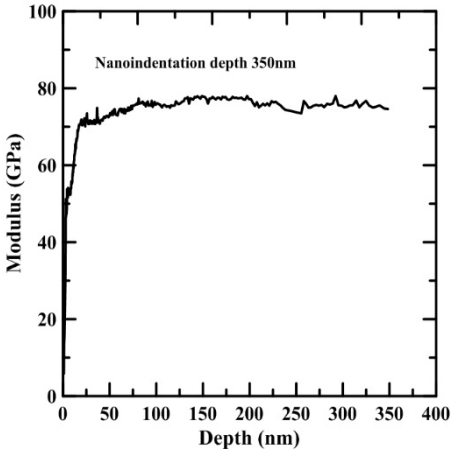

Fig. 6 (c) Modulus-displacement curves obtained in nanoindentation tests for as-deposited specimen with 200 nm thickness and indentation depth of 350 nm.

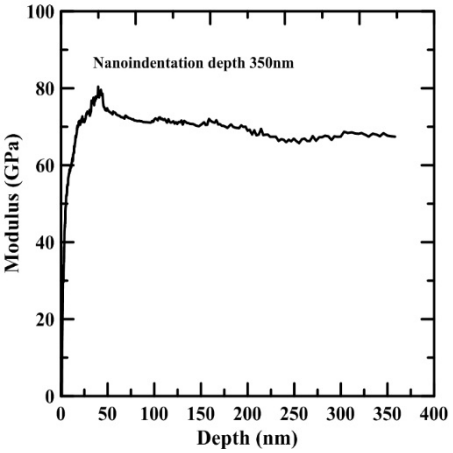

Fig. 6 (d) Modulus-displacement curves obtained in nanoindentation tests for annealed specimen with 200 nm thickness and indentation depth of 350 nm.

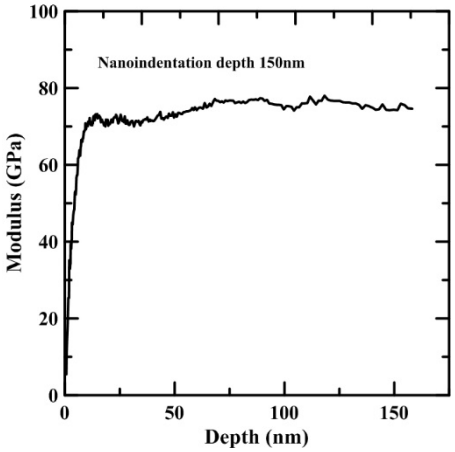

Fig. 7 (a) Modulus-displacement curves obtained in nanoindentation tests for as-deposited specimen with 300 nm thickness and indentation depth of 150 nm.

Figures 6 (c) and (d) show the variation of the Young's modulus with the indentation depth for samples with the same film thickness of 200nm but a higher indentation depth of 350 nm. The tendencies of Young's modulus of the two samples are similar to those of the samples indented to a lower depth of 150 nm. In other words, for a constant film thickness, the Young's modulus is insensitive to the depth of indentation. However, for both indentation depths, Young's modulus of annealed specimens was slightly lower than that of deposited specimens.

Figures 7(a) and (b) show the variation of the Young's modulus with the indentation depth for the as-deposited and annealed specimens, respectively, with a film thickness of 300 nm and an indentation depth of 150 nm. Figures 7(c) and (d) show the equivalent results for a higher indentation depth of 350 nm.

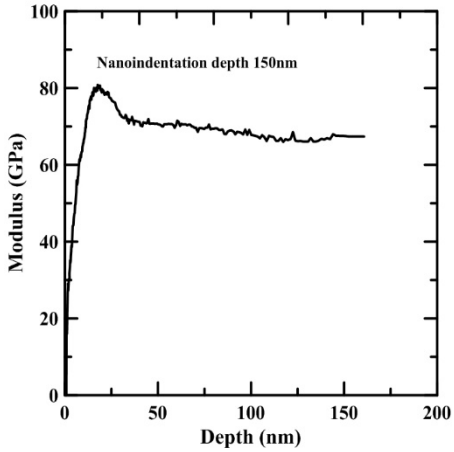

Fig. 7 (b) Modulus-displacement curves obtained in nanoindentation tests for annealed specimen with 300 nm thickness and indentation depth of 150 nm.

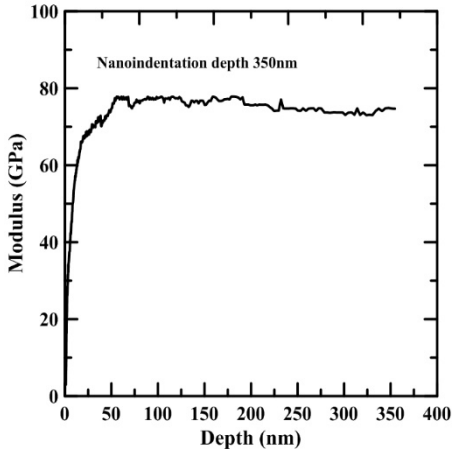

Fig. 7 (c) Modulus-displacement curves obtained in nanoindentation tests for as-deposited specimen with 300 nm thickness and indentation depth of 350 nm.

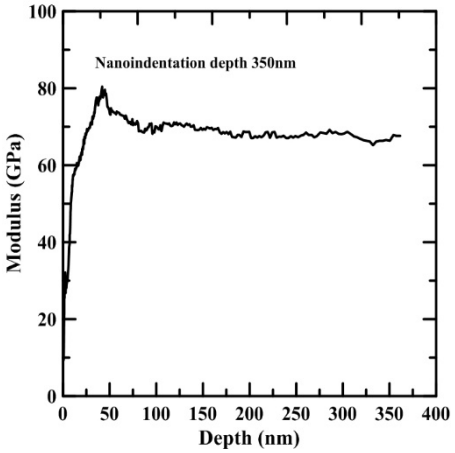

Fig. 7 (d) Modulus-displacement curves obtained in nanoindentation tests for annealed specimen with 300 nm thickness and indentation depth of 350 nm.

Figures 7 (c) and (d) show equivalent results for the higher indentation depth of 350 nm. The modulus profile in Figs. 7 (c) and (d) are similar to those in Figs. 7 (a) and (b), respectively. In other words, for a thin film thickness of 300 nm, Young's modulus is insensitive to the depth of indentation. Moreover, Young's modulus profile shown in Fig. 7 for a thin film thickness of 300 nm is similar to that shown in Fig. 6 for a film thickness of 200 nm. In other words, Young's modulus is also insensitive to the thickness of the thin film. However, for all of the samples, the annealing process resulted in a slight reduction in Young's modulus.

TEM analysis

Figures 10 (a) and (b) present TEM micrographs of the as-deposited and annealed specimens, respectively, with a film thickness of 200 nm and an indentation depth of 150 nm. A well-defined boundary is observed between the SiO_2 film and the GaAs substrate in both cases.

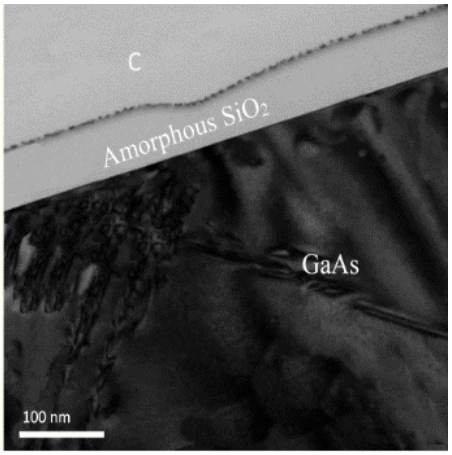

Fig. 10 (a) Micrographs of indented as-deposited specimen with 200 nm thickness and indentation depth of 150 nm obtained by TEM.

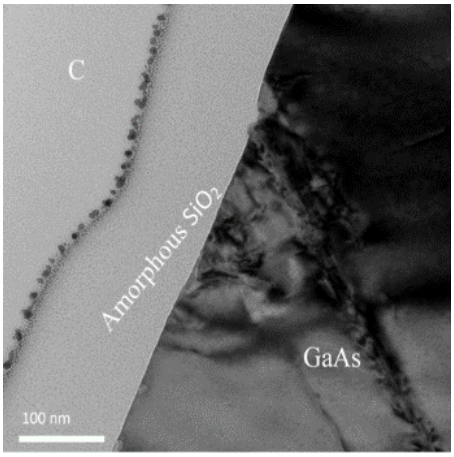

Fig. 10 (b) Micrographs of indented annealed specimen with 200 nm thickness and indentation depth of 150 nm obtained by TEM.

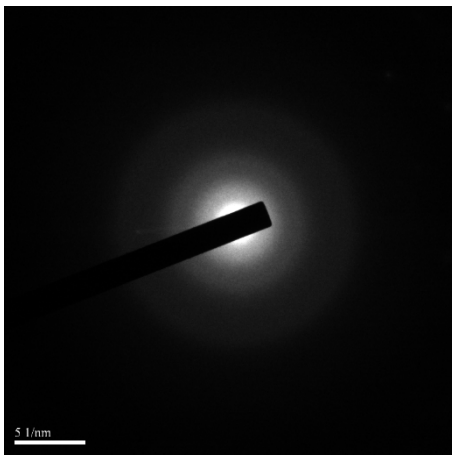

Fig. 10 (c) Selected area electron diffraction (SAED) patterns of SiO_2 film.

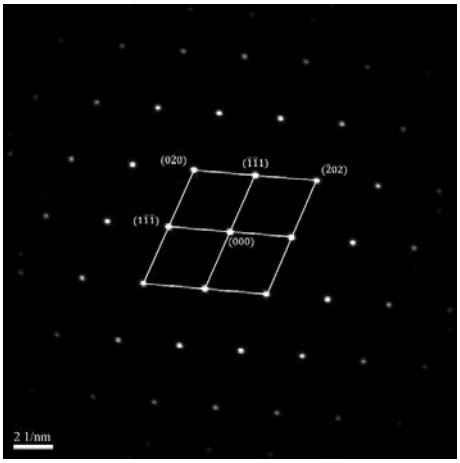

Fig. 10 (d) Selected area electron diffraction (SAED) patterns of GaAs substrate.

As shown in the selected area (electron) diffraction (SAED) pattern in Fig. 10 (c), the as-deposited and annealed SiO_2 film has an amorphous structure, while the GaAs substrate has a single crystal structure (Fig. 10 (d)).

Figures 10 (e) and (f) present high-resolution TEM (HRTEM) micrographs of the as-deposited and annealed SiO_2 thin film and GaAs substrate, respectively. There is no lattice spacing for the SiO_2 thin film since it has an amorphous structure while for the GaAs substrate is found to be around 0.283 nm, which are close to the values reported by (Kim *et al*., 1988).

Figures 11 (a) and (b) show the TEM micrographs of the as-deposited and annealed samples, respectively, with the same film thickness of 200 nm but a higher indentation depth of 350 nm. It is seen that the amorphous structure of the SiO_2 film and crystal structure of the GaAs substrate are similar to those of the samples indented to a lower depth of 150 nm. However, a delamination effect is observed at the interface between the SiO_2 film and the GaAs substrate in the as-deposited condition and the annealed condition under the higher indentation depth of 350 nm.

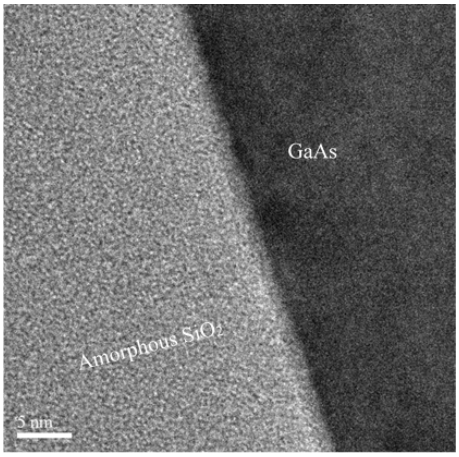

Fig. 10 (e) High-resolution TEM (HRTEM) micrographs of: SiO_2 film.

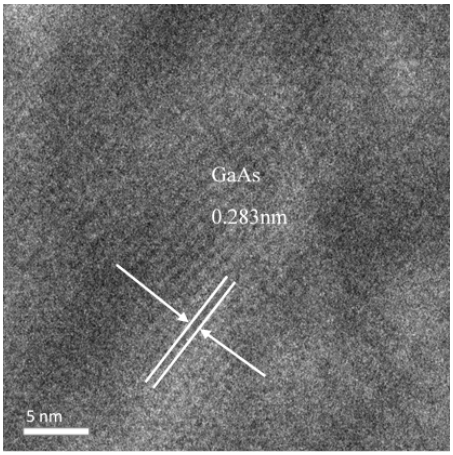

Fig. 10 (e) High-resolution TEM (HRTEM) micrographs of: GaAs substrate.

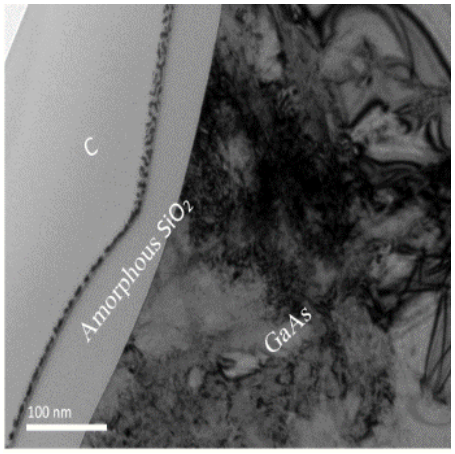

Fig. 11 (a) Micrographs of indented as-deposited specimen with 200 nm thickness and indentation depth of 350 nm obtained by TEM.

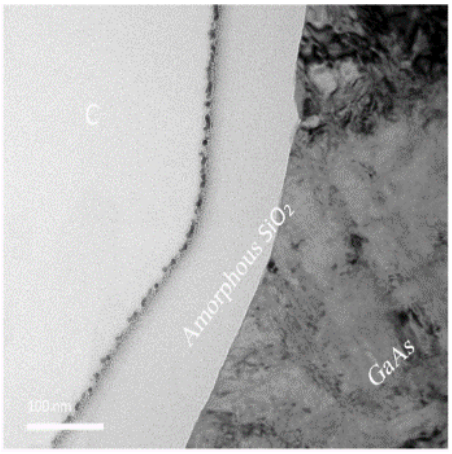

Fig. 11 (b) Micrographs of indented annealed specimen with 200 nm thickness and indentation depth of 350 nm obtained by TEM.

Figures 12(a) and (b) show the TEM micrographs of the as-deposited and annealed samples, respectively, with a thickness of 300 nm and an indentation depth of 150 nm. Figures 12(c) and (d) present the equivalent micrographs for a greater indentation depth of 350 nm.

As shown, the SiO_2 film again has an amorphous structure, whereas the GaAs substrate has a single crystal structure. However, compared to thin films with a thickness of 200 nm, delamination only occurred in the deposited specimens and became more severe with increasing indentation depth. Finally, dislocation clusters are observed only on the GaAs substrate of the annealed specimens indented to a maximum depth of 350 nm. Overall, the results presented in Figs. 11 and 12 show that the delamination behaviour strongly depends on the indentation depth, the thin film thickness, and the annealing conditions.

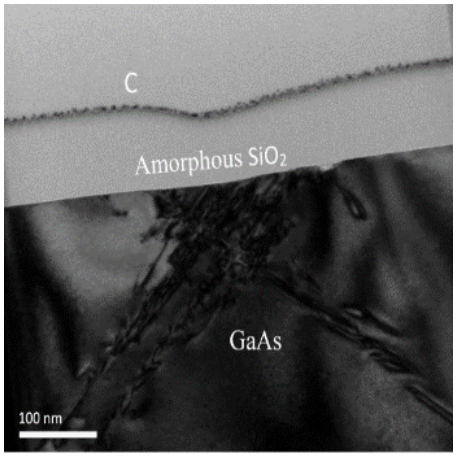

Fig. 12 (a) Micrographs of indented as-deposited specimen with 300 nm thickness and indentation depth of 150 nm obtained by TEM.

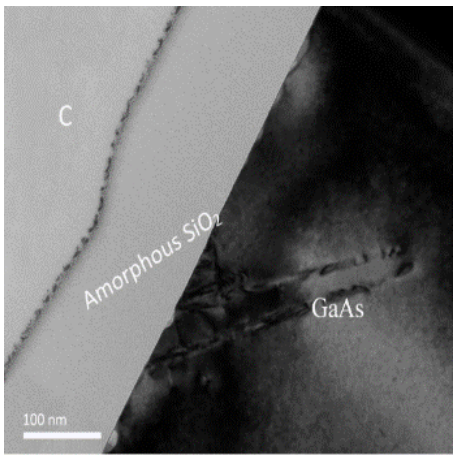

Fig. 12 (b) Micrographs of indented annealed specimen with 300 nm thickness and indentation depth of 150 nm obtained by TEM.

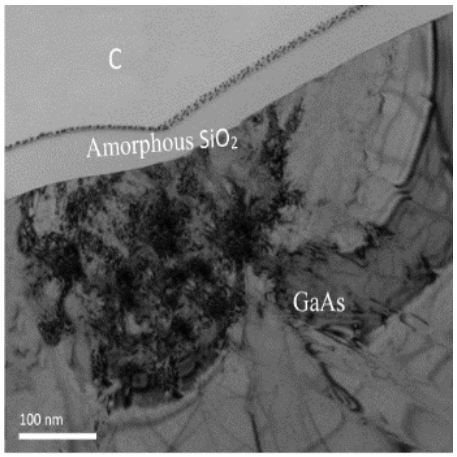

Fig. 12 (c) Micrographs of indented as-deposited specimen with 300 nm thickness and indentation depth of 350 nm obtained by TEM.

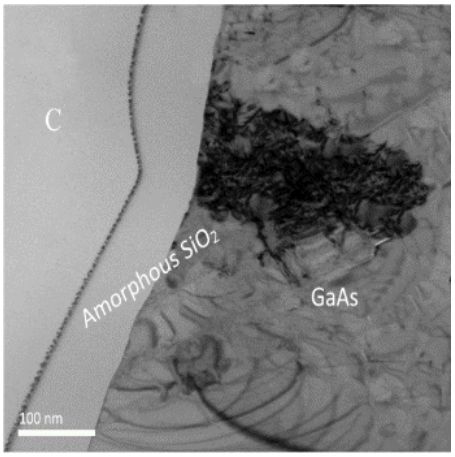

Fig. 12 (d) Micrographs of indented annealed specimen with 300 nm thickness and indentation depth of 350 nm obtained by TEM.

CONCLUSIONS

This study has investigated the nanoindentation behaviour of as-deposited and annealed SiO_2/GaAs thin-film systems with film thicknesses of 200 nm and 300 nm, respectively, and various indentation depths in the range of 150 nm to 350 nm. The results show that a pop-in event occurs in the loading curve of all the as-deposited specimens, regardless of the film thickness or indentation depth. However, for the annealed specimens, the loading curves are all smooth and continuous with no pop-in features. For both the as-deposited specimens and the annealed specimens, the maximum load increases with an increasing film thickness and the indentation depth. Furthermore, the hardness and Young's modulus are insensitive to the film thickness and indentation depth but decrease slightly following annealing. The TEM observations have revealed that delamination occurs at the interface between the SiO_2 film and the GaAs substrate for all of the samples other than the annealed samples with a thin film thickness of 300 nm. Dislocations within the GaAs substrate microstructure can be observed less obvious in the annealed sample for both two sets of the specimen. The SAED patterns have revealed that the as-deposited and annealed SiO_2 film has an amorphous structure, whereas the GaAs substrate has a single crystal structure. Finally, the high-resolution TEM (HRTEM) images have shown that the SiO_2 film doesn't have lattice spacing since it has an amorphous structure and GaAs substrate has lattice spacing of 0.283 nm.

.

ACKNOWLEDGMENT

The authors gratefully acknowledge the financial support provided to this study by the Ministry of Science and Technology (MOST) of Taiwan under Contract No. MOST 109-2221-E-239-032-MY2.

REFERENCES

A. J. Haq, P. Munroe, M. Hoffman, P. Martin, and A. Bendavid, "Deformation behaviour of DLC coatings on (111) silicon substrates," *Thin Solid Films*, vol. 516, no. 2-4, pp. 267-271, 2007.

D. Chrobak, K. Nordlund, and R. Nowak, "Nondislocation origin of GaAs nanoindentation pop-in event," *Phys Rev Lett*, vol. 98, p. 045502, Jan 26 2007.

G. Huajian, C. Cheng-Hsin, and L. Jin, "Elastic contact versus indentation modeling of multi-layered materials," *International Journal of Solids and Structures*, vol. 29, pp. 2471-2492, 1992.

G. M. Pharr, W. C. Oliver, and F. R. Brotzen, "On the generality of the relationship among contact stiffness, contact area, and elastic modulus during indentation," *Journal of Materials Research*, vol. 7 No.3, 1992.

G. Patriarche, E. Le Bourhis, D. Faurie, and P. O. Renault, "TEM study of the indentation behaviour of thin Au film on GaAs," *Thin Solid Films*, vol. 460, pp. 150-155, 7/22/ 2004.

H. S. Leipner, D. Lorenz, A. Zeckzer, H. Lei, and P. Grau, "Nanoindentation pop-in effect in semiconductors," *Physica B: Condensed Matter*, vol. 308–310, pp. 446-449, 12// 2001.

Int.J.Electrochem, "Effect of Double Layer (SiO2/TiO2) Anti-reflective Coating on Silicon Solar Cells", *Sci*., 9 (2014) 7865 – 7874.

I. Manika and J. Maniks, "Size effects in micro- and nanoscale indentation," *Acta Materialia*, vol. 54, pp. 2049-2056, 2006.

K. K. Bum, "Interfacial reactions in the Ti/GaAs system," *Journal of Vacuum Science & Technology A: Vacuum, Surfaces, and Films*, vol. 6, no. 3, p. 1473, 1988.

K. Wasmer, R. Gassilloud, J. Michler, and C. Ballif, "Analysis of onset of dislocation nucleation during nanoindentation and nanoscratching of InP," *Journal of Materials Research*, vol. 27, no. 01, pp. 320-329, 2011.

M. Hansen and K. Anderko, "Constitution of Binary Alloys," *2nd ed.McGraw-Hill, N. Y.* (1958) 51.

R. Rao, J. E. Bradby, S. Ruffell, and J. S. Williams, "Nanoindentation-induced phase transformation in crystalline silicon and relaxed amorphous silicon," *Microelectronics Journal*, vol. 38, pp. 722-726, 2007.

S. Timoshenko and J. N. Goodier, "Theory of Elasticity," *2nd ed. McGraw-Hill, N. Y.*, 1951.

S. Yugang, K. Seiyon, A. Ilesanmi, and R. J. A, "Bendable GaAs metal-semiconductor field-effect transistors formed with printed GaAs wire arrays on plastic substrates," *Applied Physics Letters*, vol. 87, p. 083501, 2005.

T. Nakamura, "Mars Rover power system for solar and laser beam Utilization," *Concepts and Approaches for Mars Exploration*, 2012.

W. C. Oliver and G. M. Pharr, "An improved technique for determining hardness and elastic modulus using load and displacement sensing indentation experiments," *Journal of Materials Research*, vol. 7, pp. 1564-1583, 1992.
X. Li and B. Bhushan, "A review of nanoindentation continuous stiffness measurement technique and its applications," *Materials characterization*, vol. 48, no. 1, pp. 11-36, 2002.
Z. Shude, Y. Yue, "Application of Silicon Oxide on High Efficiency Monocrystalline Silicon PERC Solar Cells", 2019.

退火在二氧化矽/砷化鎵薄膜奈米壓痕行為上之效應分析

李偉賢　朱威澤
國立成功大學機械工程學系

摘要

本研究主要探討退火在二氧化矽/砷化鎵薄膜之奈米壓痕行為與薄膜顯微結構上的效應。本實驗先利用電子束蒸鍍法在砷化鎵晶圓上製作200 nm及300nm厚度之二氧化矽薄膜後，經過退火處理，其條件為加熱至500℃並持溫30分鐘，再將試片進行深度為150nm 及 350 nm之奈米壓痕試驗，藉此探討退火對奈米壓痕行為及微觀結構之影響。奈米壓痕實驗結果顯示，硬度及楊氏模數受退火影響甚鉅，未退火與退火後之硬度-深度曲線有很大的不同，退火後的硬度值較未退火低，而楊氏模數則具有相同的趨勢；負載-深度曲線顯示，在對薄膜厚度為200nm及300nm之試片進行150nm 及350 nm壓痕深度時，退火與未退火的荷載曲線皆有pop-in現象發生。穿透式電子顯微鏡之觀測結果證實，薄膜與基材分離僅發生在膜厚300 nm，壓深150 nm與350 nm的條件，而在兩組退火後試片中，皆可觀察到微結構內的差排不太明顯。在結構分析的部分，可以觀察出SiO2薄膜為非晶結構，而GaAs屬於單晶結構。最後於高解析穿透式電子顯微鏡分析結果顯示，因為SiO2薄膜屬於非晶結構故無晶格間距，而GaAs 基材的晶格間距為0.283nm。